

On amplitude beam splitting of tender X-rays (2–8 keV photon energy) using conical diffraction from reflection gratings with laminar profile

Werner Jark* and Diane Eichert

X-ray Fluorescence Beamline, Elettra – Sincrotrone Trieste ScpA, SS 14, km 163.5 in Area Science Park, Basovizza, 34149 Trieste, Italy. *Correspondence e-mail: werner.jark@elettra.eu

Received 6 July 2015

Accepted 19 October 2015

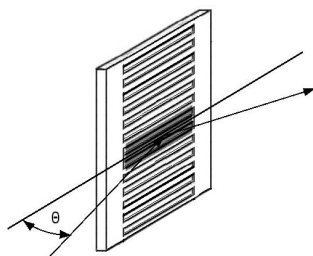
Edited by D. Cocco, SLAC National Accelerator Laboratory, USA

Keywords: diffraction grating; laminar profile; beam splitter; X-rays.

Conical diffraction is obtained when a radiation beam impinges onto a periodically ruled surface structure parallel or almost parallel to the ruling. In this condition the incident intensity is diffracted through an arc, away from the plane of incidence. The diffracted intensity thus lies on a cone, which leads to the name ‘conical diffraction’. In this configuration almost no part of the ruled structure will produce any shadowing effect for the incident or the diffracted beam. Then, compared with a grating in the classical orientation, relatively higher diffraction efficiencies will be observed for fewer diffraction orders. When the incident beam is perfectly parallel to the grooves of a rectangular grating profile, the symmetry of the setup causes diffraction of the intensity symmetrically around the plane of incidence. This situation was previously tested experimentally in the VUV spectral range for the amplitude beam splitting of a radiation beam with a photon energy of 25 eV. In this case the ideally expected beam splitting efficiency of about 80% for the diffraction into the two first orders was confirmed for the optimum combination of groove depth and angle of grazing incidence. The feasibility of the amplitude beam splitting for hard X-rays with 12 keV photon energy by use of the same concept was theoretically confirmed. However, no related experimental data are presented yet, not even for lower energy soft X-rays. The present study reports the first experimental data for the conical diffraction from a rectangular grating profile in the tender X-ray range for photon energies of 4 keV and 6 keV. The expected symmetries are observed. The maximum absolute efficiency for beam splitting was measured to be only about 30%. As the reflectivity of the grating coating at the corresponding angle of grazing incidence was found to be only of the order of 50%, the relative beam splitting efficiency was thus 60%. This is to be compared also here with an ideally expected relative efficiency of 80%. It is predicted that a beam splitting efficiency exceeding 50% should be possible by use of more appropriate materials.

1. Introduction

When reflection gratings are used for the monochromatization of soft X-rays with photon energies up to and above 1000 eV at synchrotron radiation sources, the choice falls always to gratings with grooves of either rectangular or of sawtooth shape with very shallow inclination angle (*e.g.* Hutley, 1982). The former are also referred to as laminar gratings, while the latter are denoted blazed gratings. Their respective profiles are shown in Fig. 1. Appreciable diffraction efficiency will be found only when the grating is operated in the total reflection regime of the coating material. Thus the angle of grazing incidence needs to be smaller than the critical angle. As first discussed by Lukirskii & Savinov (1963), when applying such small angles, part of the structured surface will not be illuminated when the beam follows the trajectory in the classical



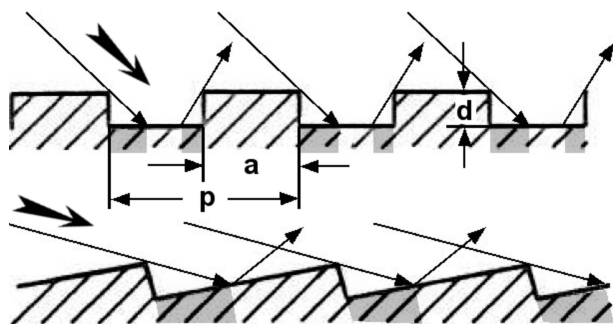


Figure 1
Shadowing effects when laminar (top) and sawtooth (bottom) grating profiles are illuminated at very shallow angles of incidence. The shaded areas do not participate in the diffraction into the indicated direction for the exiting rays. The grating periodicity is p , while the tops in the rectangular profile have width a and the groove depth is d .

orientation, as shown in Fig. 1 and on the left in Fig. 2. As presented at the top of Fig. 1, the valleys of the rectangular grooves remain partly in the shadow for two reasons: the incident beam cannot illuminate the related shaded areas, and an observer behind the grating cannot receive the reflected intensity from them. The situation seems to be more favorable in the blazed profile, shown at the bottom of Fig. 1, as all incident photons will hit areas which can reflect or diffract the beam to an observer. In fact, the grating could be operated such that one of the diffraction orders would be specularly reflected at the grooves, which is the so-called blaze maximum mode (e.g. Hutley, 1982). Nevertheless, neither in this blazed profile nor in the laminar profile can the diffracted intensity be confined exclusively in a single peak. Maystre & Petit (1976) observed phenomenologically in their theoretical predictions that the reduction of the efficiency for first-order diffraction from the blazed profile and the redistribution of the intensity into other orders is directly dependent on the relative amount of shadow regions in the diffracted beam. This observation is confirmed in experiments reported by Jark (1988). This disturbing shadowing effect can be eliminated when the grating is rotated by 90° around the surface normal to the extreme off-plane orientation, which was used for the first

time by Greig & Ferguson (1950). Then, in the blazed profile for a particular order, the beam could still be reflected specularly at the entire surface of the now inclined grooves. Relatively high diffraction efficiencies have already been found experimentally in this advantageous configuration by Werner (1977) for the soft X-ray range up to photon energies of 1.56 keV. Successively, Neviere *et al.* (1978) initiated the related theoretical treatment. Successful tests led to the use of conical diffraction in spectrographs, for the lower energy part of the soft X-rays, to be operated in space crafts (Cash, 1982; McEntaffer *et al.*, 2013) as well as to use in the VUV/EUV spectral region in combination with incident beams from lasers or plasmas (see, for example, Frassetto *et al.*, 2014, and references therein). For use in monochromators at synchrotron radiation sources, only two design studies, but no practical realisations, have been reported. The instrument described by Werner & Visser (1981) covered the soft X-ray range up to 2 keV photon energy, while the concept of Koike & Namioka (2004) covered larger photon energies between 1 keV and 4 keV in the tender X-ray range.

Any substantial shadowing can also be avoided in the extreme off-plane orientation in the rectangular profile, which is shown on the right in Fig. 2. However, differently to the blazed profile, this configuration is highly symmetric for the incident beam, and thus the diffraction is expected to be symmetric as well with respect to both the diffracted intensity distribution and the peak positions. It is possible, by proper choice of the ruling parameters, as discussed by Braig *et al.* (2012), to concentrate the diffracted intensity mostly and equally into two symmetrically oriented peaks. This symmetric diffraction in a laminar grating was tested in the VUV range for a photon energy of 25 eV and it was fruitfully applied by Braig *et al.* (2012) for use in an amplitude beam splitter. The feasibility of this application for larger photon energies of the order of 12 keV was theoretically investigated by Goray (2008) and confirmed. However, no related experimental verification of the latter has been reported so far. In fact, no experimental data are reported yet related to the diffraction efficiency of reflection gratings in the extreme off-plane orientation for the entire tender X-ray range (2–8 keV), neither for the laminar nor for the blazed profile. Instead, as an example of the classical orientation, Cocco *et al.* (2007) report data for photon energies between 2 keV and 6 keV. They found relatively small efficiencies for on-blaze operation, which decrease from 10% to 5%, respectively.

The present study will address the performance of the rectangular profile grating when it is operated in conical diffraction for diffracting in this range of tender X-rays.

2. Experimental details

2.1. Grating properties

The data reported here deal with X-rays with photon energies of $E = 4$ keV and $E = 6$ keV (X-ray wavelength $\lambda = 0.31$ nm and 0.207 nm, respectively). The investigated structure is a holographically prepared reflection grating with

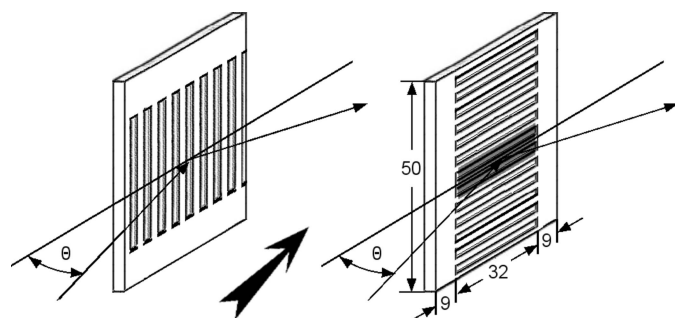


Figure 2
Laminar grating profiles oriented for horizontal beam deflection. The classical orientation is shown on the left, while the extreme off-plane orientation is shown on the right. The latter figure reports the dimensions of the substrate and of the structured area. The shaded area indicates the maximum possible footprint length.

rectangular grooves of period $p = 820 \text{ nm}$ ($1220 \text{ lines mm}^{-1}$). The widths of the tops ($a = 370 \text{ nm}$) and of the valleys (450 nm) were slightly different with the tops filling $a/p = 0.45$ of the periodicity. The valleys were etched to a depth of about $d = 7 \text{ nm}$ into a silicon carbide substrate ($50 \text{ mm} \times 50 \text{ mm}$). As shown in Fig. 2, the grooves covered the entire substrate length, but they were only 32 mm wide. Accordingly, two stripes of 9 mm width and 50 mm length remained unstructured to the side of the grooves. After the etching the entire substrate was coated with a gold layer of thickness 30 nm on a thin chromium binding layer. A prototype object was proposed and tested to withstand the heat load at Elettra soft X-ray undulators (Jark, 1992). Consequently the substrate is suitable for high-power sources. However, when the grating is utilized at X-ray free-electron lasers (XFELs) (Emma *et al.*, 2010), according to Barkusky *et al.* (2010) better materials than gold with a relatively small damage threshold for the single shots emitted by XFELs will have to be employed.

2.2. Experimental setup in an X-ray reflectometer

The test was performed at the X-ray fluorescence beamline at Elettra, where the sample was installed in a seven-axis diffractometer, described by Lubeck *et al.* (2013), which is operated in a vacuum chamber. The sample was oriented for horizontal beam deflection as shown in Figs. 2 and 3. The double-crystal monochromator (Jark *et al.*, 2014) provides a relative spectral bandwidth of about 0.014% in the hard X-ray range. It is operated in combination with a double-mirror higher-order suppressor. At the sample position the beam has a top-hat profile with width 0.25 mm in the horizontal plane of incidence and height 0.12 mm perpendicular to it (*i.e.* in the vertical plane). The intrinsic beam angular spread in both directions is 0.13 mrad . In the vacuum chamber the reflected/diffracted intensity can be registered by use of a photodiode detector (Hamamatsu Si-photodiode S3590-09) at a distance of 0.14 m from the sample. The beam acceptance is limited in the horizontal plane of incidence as shown in Fig. 3 by a

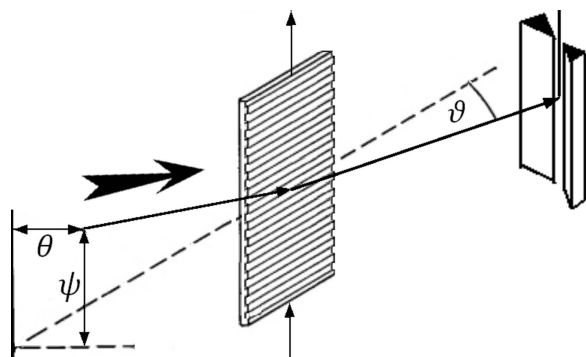


Figure 3

Orientation of the laminar grating and of the detector slit in the experiment, in which the angle of grazing incidence θ and the azimuthal orientation angle ψ of the grating grooves were fixed. Then either an image was taken using a CCD camera or the intensity diffracted into the angle of grazing exit ψ was registered by scanning a diode detector with an entrance slit in the respective direction.

vertical slit of opening 0.2 mm , which provides an angular resolution of 1.43 mrad (0.08°).

Two-dimensional profiles of the beam downstream of the sample could be registered by use of a CCD camera (PCO Sencam qe with pixel size $6.7 \mu\text{m}$) with X-ray converter screen and transfer optics. This system was operated at 0.55 m from the sample in air behind a beryllium exit window.

In the extreme off-plane orientation the ruled length of the grooves of 32 mm , as shown on the right in Fig. 2, can intercept the entire beam footprint only for larger angles of grazing incidence, $\theta > 0.46^\circ$ (7.8 mrad).

2.3. Coordinate system for the diffraction peak positioning

In the off-plane grating configuration one finds that the incident radiation is diffracted through an arc, and thus the diffracted intensity is found on a cone with opening angle γ as shown in Fig. 4 (top), which leads to the description of ‘conical diffraction’ (Werner, 1977). The exit cone remains stationary

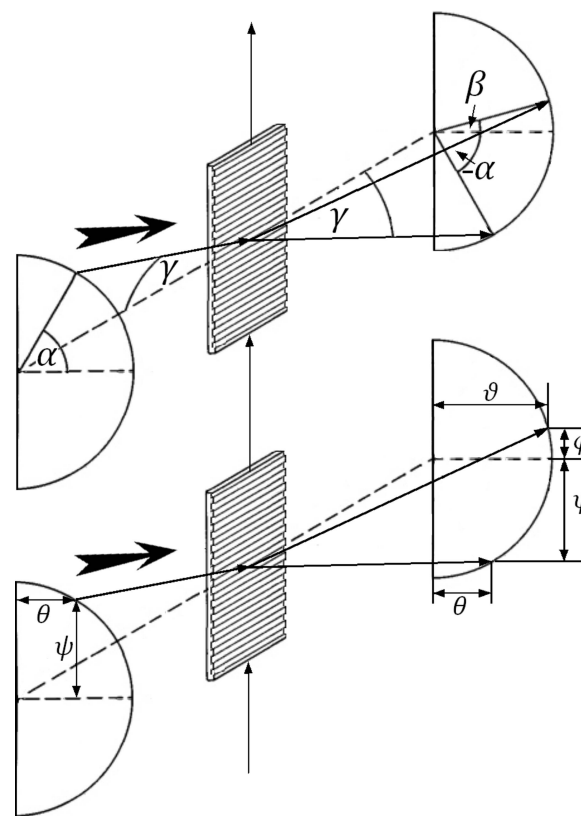


Figure 4

Orientation of the laminar grating close to the extreme off-plane configuration for horizontal beam deflection. The drawing is not shown to scale. The X-rays travel from left to right. For any source point on the left semi-arc all diffracted orders will be found on the right semi-arc with identical opening angle γ . The upper figure presents the angle convention as usually used in connection with the off-plane configuration, with α and β being the orientation angles on the arc of the incident and of the diffracted beam, respectively. In the lower figure rectangular coordinates are used. The angle of grazing incidence is denoted θ , while the orientation angle of the grooves with respect to the specularly reflected beam is ψ . φ and ϑ are the positions of a diffracted order with respect to the plane, which is perpendicular to the surface and parallel to the grooves.

as long as the incident beam falls onto a cone with the same opening angle γ and in line with the exit cone. For monochromatic radiation with wavelength λ the azimuthal position angles β_m of the diffracted orders on the cone are most conveniently given in spherical coordinates, as discussed by Werner (1977),

$$\sin \gamma (\sin \alpha + \sin \beta_m) = m\lambda/p, \tag{1}$$

where α is the position angle of the source, m is the diffraction order number, which increases counterclockwise, and p is the grating periodicity. In the study reported here with a configuration operated as shown in Fig. 3, the diffractometer permitted to vary independently the angle of grazing incidence θ onto the grating surface and the orientation angle ψ between the beam trajectory projected onto the grating surface and the orientation of the grooves. The blades of the slit in front of the photodiode detector were parallel to the grating surface as shown in Fig. 3. In this case only the angle of grazing exit ϑ intercepted by the detector could be varied. The CCD camera was oriented such that its columns were parallel to the blades of the slit in front of the photodiode. For the indicated motions it is then more convenient to discuss the experimental data in rectangular coordinates as shown at the bottom of Fig. 4. Both orientation angles θ and ψ are rather small and one can thus use

$$\sin \gamma = (\psi^2 + \theta^2)^{1/2}. \tag{2}$$

The reference for the diffracted orders is now the plane, which is parallel to the grooves and perpendicular to the grating surface.

One will then find the diffraction peaks at the rectangular coordinates

$$\varphi_m = m \frac{\lambda}{p} - \psi \tag{3}$$

and

$$\vartheta_m = \left[\theta^2 + 2m \frac{\lambda}{p} \psi - \left(m \frac{\lambda}{p} \right)^2 \right]^{1/2}. \tag{4}$$

Equation (3) indicates that all orders line up at equidistant positions in angle $\Delta\varphi$. This angle depends neither on θ nor on ψ . Then the peaks of equal order m but opposite sign are found at symmetric distances in the vertical direction from the order $m = 0$. In the horizontal direction instead one finds unaltered positions for the diffraction peaks, when the signs for m and ψ are reversed.

3. Discussion of experimental data

3.1. Conical diffraction in images taken at a photon energy of 6 keV

The grating was aligned to the extreme off-plane orientation by fixing the angle of grazing incidence θ and by successively rotating ψ until the orders were oriented symmetrically around the position for $m = 0$. This was defined as the position with nominally $\psi = 0^\circ$. The error is smaller than $\Delta\psi = 0.05^\circ$, as

such a misalignment already produced a visibly appreciable asymmetry. The three exposures with increment $\Delta\psi = 0.5^\circ$ around the symmetry position are shown at the top of Fig. 5 for 6 keV photon energy and for an angle of grazing incidence of $\theta = 0.5^\circ$. For the angular setting with $\theta > 0.46^\circ$ the grooves intercepted the entire incident beam. The measured peak width of 0.3 mm at the CCD in the horizontal direction corresponds to an opening angle of about 0.55 mrad (0.03°). The nine exposures in the lower part are taken at the same

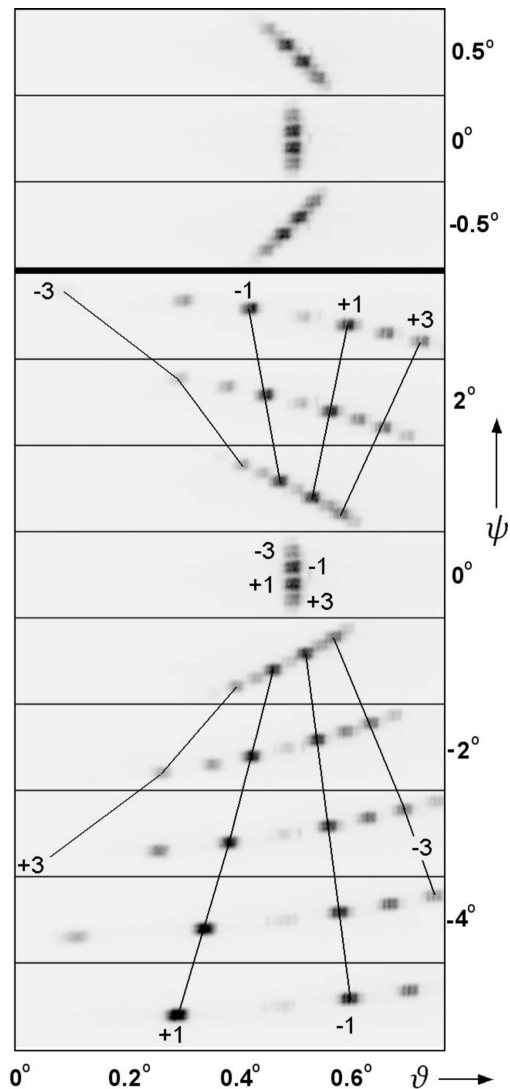


Figure 5 Images taken using the CCD camera of the diffracted intensity as a function of the angle of grazing exit ϑ for varying grating orientation angle ψ in linear grey code (black is maximum intensity). The upper three images refer to the positions around perfect alignment to the extreme off-plane orientation (step size $\Delta\psi = 0.5^\circ$) for a photon energy of 6 keV and an angle of grazing incidence of $\theta = 0.5^\circ$. The size of the diffraction peaks is about 0.3 mm horizontally and 0.26 mm vertically and each single image (1108 pixels horizontally \times 224 pixels vertically) covers in the vertical direction an angular interval of $\Delta\varphi = 0.15^\circ$, which corresponds to the separation between the diffraction peaks with indices $m = 5$ and $m = -5$. The step size is increased in the lower nine pictures to $\Delta\psi = 1^\circ$. The more intense odd orders ($-3, -1, +1$ and $+3$) are labelled and connected by lines as guides for the eye.

angle of grazing incidence, $\theta = 0.5^\circ$, but now with a larger increment, $\Delta\psi = 1^\circ$, in the range $\psi = -5^\circ$ (bottom) and $\psi = 3^\circ$ (top). The more intense odd orders are labelled with their order numbers. One finds the expected symmetries for the intensity distributions and for the peak positions as discussed for the predictions according to (3) and (4). As predicted in (3), upon changing the grating orientation angle ψ a diffraction peak of a given order m does not move in the vertical direction but only in the horizontal direction. The zeroth order was expected to remain stationary, and thus its small lateral motion indicates some residual cross-talk introduced into the θ rotation, when the ψ orientation is varied. This small drift remained negligible for the scope of data interpretation and it was thus not compensated.

3.2. Diffraction efficiency for the laminar grating profile in conical diffraction

In Fig. 5 (top) one can easily recognize that only a few orders receive significant diffracted intensity. While the zeroth order is almost absent, the two symmetrically oriented first orders ($m = +1$ and $m = -1$) receive in this case almost half of the diffracted intensity. For smaller angles $|\psi| \leq 1^\circ$ the third orders receive more intensity than the second orders. In detail it is found that for the chosen angle of grazing incidence of $\theta = 0.5^\circ$ the total diffracted intensity is 53% of the incident intensity, while 47% of the diffracted intensity is contained in the two first orders. Consequently each first order contains 12.5% of the incident intensity. This latter number confirms nicely the efficiency advantage in the off-plane orientation compared with the classical orientation. In fact, the efficiency improvement is more than twofold compared with the efficiency from a more favorable blazed grating, as measured by Cocco *et al.* (2007) in the classical orientation. The latter could be operated in blaze maximum below the critical angle for total reflection only for the smaller groove density of 600 mm^{-1} .

Here it was also possible to measure the reflected intensity from the unruled stripe of width 9 mm and length 50 mm for the same angle in the classical orientation as shown on the left in Fig. 2. The latter reflectivity was identical to the total diffracted intensity from the structured area. Consequently one has to assume that both the tops and the valleys of the ruled profile reflected the incident intensity like mirrors, as one would have ideally expected. Then the system can be looked at as two interwoven systems of periodic plane stripes with identical reflectivity. In the transmitted intensity one will observe interference, as between the reflected beams from adjacent stripes an optical path difference (OPD) is found due to the increased optical path through the valleys. The OPD is

$$\text{OPD} = 2d \sin \theta, \quad (5)$$

which produces a retardation in phase by

$$\frac{2\pi \text{OPD}}{\lambda} = \frac{4\pi d}{\lambda} \sin \theta. \quad (6)$$

The interference in this situation is discussed in a very general form by Born & Wolf (1980), and in a more adapted form for

the present situation by Schnopper *et al.* (1977). For the present favorable condition, with finite but identical reflectivities R at the tops and in the valleys, one finds the following diffraction efficiencies for the orders:

$$\eta_{|m| \neq 0} = 2R(1 - P) \left[\frac{\sin(m\pi a/p)}{m\pi} \right]^2, \quad (7)$$

$$\eta_0 = R \left\{ \left(\frac{a}{p} \right)^2 + \left[1 - \left(\frac{a}{p} \right) \right]^2 + 2 \left(\frac{a}{p} \right) \left[1 - \left(\frac{a}{p} \right) \right] P \right\}, \quad (8)$$

where P refers to the phase retardation expressed as

$$P = \cos \left(\frac{4\pi d}{\lambda} \sin \theta \right). \quad (9)$$

As long as $0.45 < a/p < 0.55$, which covers the present grating structure, equation (8) can be approximated as

$$\eta_0 \approx 0.5R(1 + P). \quad (10)$$

For the present ratio $a/p = 0.45$, the factor c_m in equation (7),

$$c_m = \left[\frac{\sin(m\pi a/p)}{m\pi} \right]^2, \quad (11)$$

has the values $c_1 = c_{-1} = 0.099$, $c_2 = c_{-2} = 0.0024$ and $c_3 = c_{-3} = 0.0089$. This is an insignificant difference compared with the ideal ratio for $a/p = 0.5$, when $c_1 = c_{-1} = 0.101$, $c_2 = c_{-2} = 0$ and $c_3 = c_{-3} = 0.0113$. In this ideal case one finds $c = 0$ for all even orders. Then the best efficiency for $m \neq 0$ is found according to (7) when the phase retardation yields $P = -1$, and thus $\eta_0 = 0$, *i.e.* the zeroth order receives negligible diffracted intensity. This leads to $2(1 - P) = 4$ and it corresponds according to (9) and (5) to $\text{OPD} = (2n + 1)\lambda/2$ where n is an integer number. Here the ratio η_m/R can be defined to be the structural efficiency of the laminar profile. This can thus ideally be as high as $\eta_{|m|=1}/R = 0.405$. In the case that the valleys or the tops are not reflecting, then the factor $2(1 - P)$ in equation (7) reduces simply to $2(1 - P) = 1$. This leads to a rather significant fourfold drop in the structural efficiency to $\eta_{|m|=1}/R = 0.101$. In light of these results in the optimum condition the present grating could have concentrated about 80% of the diffracted intensity into the two first orders. Experimentally a value of 47% was found, which is only about 60% of the ideally expected performance. However, one has to recognize that the experiment was made with $\theta = 0.5^\circ$ and not with the optimum angle according to (9), which is predicted for the chosen wavelength $\lambda = 0.207 \text{ nm}$ (6 keV photon energy) to be $\theta = 0.43^\circ$. In this condition the grooves no longer intercept the entire beam and thus a more appropriate condition needs to be chosen.

3.3. Diffraction efficiency derived in the optimum configuration for a photon energy of 4 keV

The groove filling just discussed can be achieved with larger wavelength and consequently the diffraction efficiency was measured more carefully for a wavelength of $\lambda = 0.31 \text{ nm}$ (photon energy of 4 keV). In this case according to (3) and (4) the orders are also advantageously more separated. Conse-

quently the diffracted intensity can in this case also be measured by use of the photodiode detector, even though its limited angular resolution of 1.43 mrad (0.08°) for the horizontal direction cannot compete with the resolution provided by the CCD. In this case first the angular position θ for minimum diffraction into the zeroth order was determined by use of the CCD camera. The related angle of $\theta = 0.64^\circ$, which is consistent with the expectation according to (9), was chosen for the experiment. The distribution of the diffracted intensity was registered depending on the angle ϑ for a set of 29 angular positions ψ ($\Delta\psi = 0.5^\circ$). Fig. 6 shows the related intensity maps, normalized to the incident intensity, displayed very similarly to the CCD images in Fig. 5, with the angle ϑ in the abscissa and the angle ψ in the ordinate. Obviously the first-order peaks could not be separated in the vicinity of the extreme off-plane configuration. Thus the efficiency for the diffraction into these first orders cannot be determined directly. However, it can be extrapolated from its dependence on the angle ψ .

At this point one has to recognize that the size of the incident beam with top-hat profile of about 0.255 mm in the horizontal direction at the photodiode detector is wider than the opening of the vertical slit of 0.2 mm. One expects that, away from the specular reflection condition, in the horizontal direction the size of the footprint projected into the direction of the diffracted peaks is varying according to

$$s_m = s_0 \frac{\vartheta_m}{\theta}, \tag{12}$$

where s_0 is the size of the incident beam. As a consequence, the measured peak widths increase in the horizontal direction when the position angles ϑ_m increase, and the measured signal then refers to the flux density at any angular position. The related variation of the peak width with increasing exit angle ϑ_m is very obvious in Fig. 5. In all measured intensity distributions in which the two first orders were sufficiently separated from each other and from the higher-order peaks, they were fitted with two independent but overlapping profiles of Gaussian shape. The free parameters in the fit were the peak positions, the peak widths and the peaks heights. The positions were found to be in agreement with the predictions according to (4); likewise the fitted widths confirmed the dependence on the exit angles ϑ_{-1} and ϑ_1 according to (12). The peak heights, *i.e.* the flux densities, obtained from this procedure will be discussed in more detail. They are plotted in Fig. 7 independently for both first orders and after a normalization with respect to the incident flux density. One can now assume that the diffraction efficiency will not undergo a significant varia-

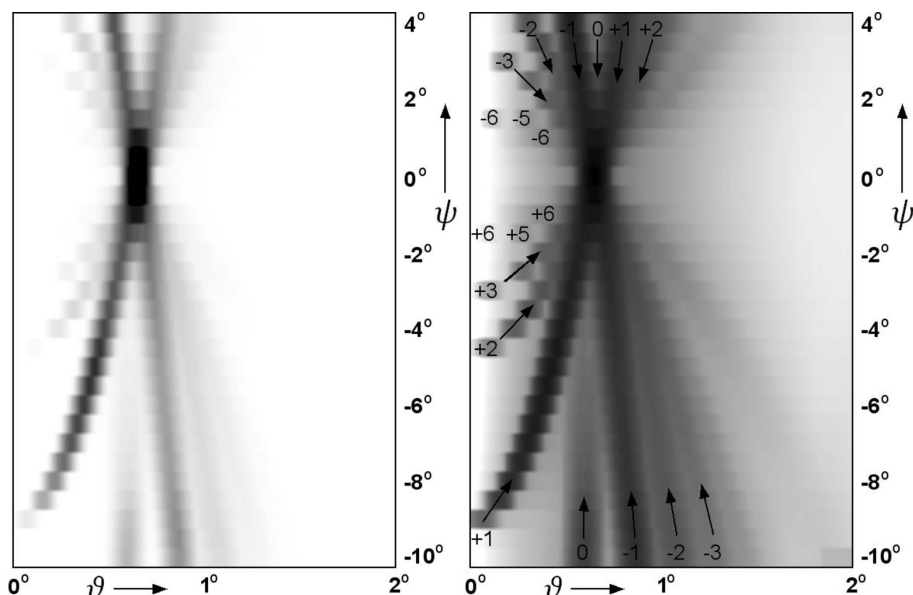


Figure 6 Left: grey-scale plot (black is maximum intensity in the linear plot on the left) of the intensity distributions of the diffracted beam as registered by the photodiode as a function of the angle ϑ (abscissa) and for 29 positions of ψ . The photon energy was 4 keV, and the angle of grazing incidence of $\theta = 0.64^\circ$ suppressed the specularly reflected peak ($m = 0$) the best. Right: the same intensities but on a logarithmic scale, which presents smaller intensities more clearly. In this plot most of the lower index orders are labelled, as are some isolated high-order peaks.

tion as long as the grooves are rotated away from the optimum orientation angle ψ by only a smaller amount, such that shadowing effects remain still negligible. Then for constant efficiency the fitted peak heights in Fig. 7 should vary according to ϑ_m/θ . The two related predictions are plotted in Fig. 7 as lines for $m = +1$ and for $m = -1$ assuming identical constant efficiencies of 0.155 for $\psi = 0^\circ$. Both curves are in

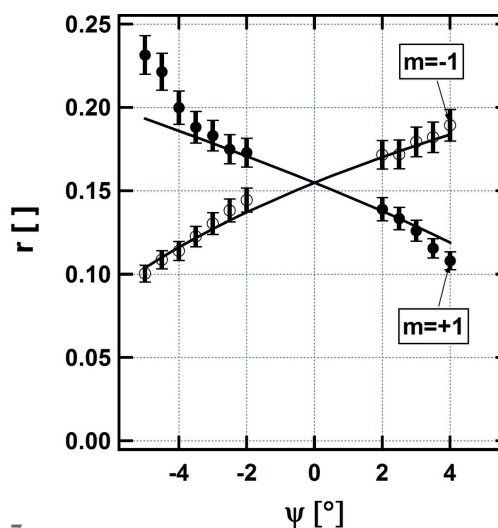


Figure 7 Peak heights, as fitted to the normalized intensity distributions in Fig. 5, for the orders with index $m = +1$ (filled circles) and with index $m = -1$ (open circles) depending on the orientation angle ψ . r is the ratio between the measured diffracted intensity and the incident intensity. The lines refer to the predictions assuming constant and identical efficiencies for the diffraction into both orders of 0.155 and a variation of the beam cross-section according to ϑ_m/θ .

good agreement with the measured data. Consequently one finds that in this case 15.5% of the incident intensity is diffracted into each first order.

Also, in this case for a photon energy of 4 keV, it was found that the reflectivity of $R = 46.5\%$ measured in the long unstructured stripe next to the ruling is identical to the total diffracted intensity from the ruling in the extreme off-plane orientation with $\psi = 0^\circ$. Consequently the relative diffraction efficiency for the structure is $\eta_{|m|=1}/R = 33\%$. This efficiency is consistently confirmed in the CCD images taken during alignment for optimum zeroth-order suppression at $\psi = 0^\circ$, in which more than 60% of the diffracted intensity was contained in the two first orders. Ideally the two related numbers could have been 40.5% for the single-order efficiency and 81% for the sum of both. Consequently the structure provides already a high structural efficiency of about 80% of the ideal expectation for beam splitting. Then in the first place it is the reflectivity R which needs to be improved in order to provide higher diffraction efficiencies. Either one chooses a more appropriate coating material or one operates the system at more grazing angles, which will eventually require deeper grooves for maintaining optimum performance according to (9). By this means a practical diffraction efficiency of the order of 25% for each first order should be within reach. Consequently the efficiency of the laminar grating profile for amplitude beam splitting in conical diffraction could be 50% or even higher.

At this point some comments need to be made related to other symmetric grating profiles. In fact, gratings with sinusoidal profile and with perfect triangular profile are operated in a perfectly symmetric situation, when put into the extreme off-plane orientation. Consequently gratings with these two profiles can be used as amplitude beam splitters. In these profiles shadowing effects can be completely avoided. Nevertheless, compared with the laminar grating both profiles have less inherent capability for the simultaneous suppression of several diffraction orders. Consequently both provide reduced beam splitting efficiency when compared with the laminar profile with identical groove density and coating.

4. Conclusion

It was shown that reflection gratings with rectangular groove profiles can be used as efficient and symmetric beam splitters for tender X-rays with photon energies of 4 keV and 6 keV, when operated in the extreme off-plane configuration. The ideally expected performance can be predicted with simple analytical equations. The present structure provided already about 80% of the expected structural efficiency. On the other hand the reflectivity of the substrate for the optimum setting was found to be only about 50%, which accordingly led to

reduced practical efficiencies. With improved reflectivity it is expected that an efficiency for the amplitude beam splitting of X-rays of the order of 50% can be achieved by use of a laminar profile reflection grating. Such objects could thus become particularly important for beam splitting at presently commissioned X-ray free-electron lasers, e.g. as the first component in delay lines (Mitzner *et al.*, 2005). For this application it is advantageous that the profile can be prepared in substrates which can withstand larger power loading.

Acknowledgements

We acknowledge the use of the experimental chamber for X-ray spectrometry of the International Atomic Energy Agency (IAEA), which is operated in partnership at the X-ray fluorescence beamline at Elettra.

References

- Barkusky, F., Bayer, A., Döring, S., Grossmann, P. & Mann, K. (2010). *Opt. Express*, **18**, 4346–4355.
- Born, M. & Wolf, E. (1980). *Principles of Optics*, ch. 8.6. New York: Macmillan.
- Braig, C., Fritzsche, L., Käsebier, T., Kley, E.-B., Laubis, C., Liu, Y., Scholze, F. & Tünnermann, A. (2012). *Opt. Express*, **20**, 1825–1838.
- Cash, W. (1982). *Appl. Opt.* **21**, 710–717.
- Cocco, D., Bianco, A., Kaulich, B., Schaefers, F., Mertin, M., Reichardt, G., Nelles, B. & Heidemann, K. F. (2007). *AIP Conf. Proc.* **879**, 497–500.
- Emma, P. *et al.* (2010). *Nat. Photon.* **4**, 641–647.
- Frassetto, F., Miotti, P. & Poletto, L. (2014). *Photonics*, **1**, 442–454.
- Goray, L. I. (2008). *J. Surface. Investig.* **2**, 796–800.
- Greig, J. H. & Ferguson, W. F. C. (1950). *J. Opt. Soc. Am.* **40**, 504–505.
- Hutley, M. (1982). *Diffraction Gratings (Techniques of Physics)*. New York: Academic Press.
- Jark, W. (1988). *Nucl. Instrum. Methods Phys. Res. A*, **266**, 414–421.
- Jark, W. (1992). *Rev. Sci. Instrum.* **63**, 1241–1246.
- Jark, W., Eichert, D., Luehl, L. & Gambitta, A. (2014). *Proc. SPIE*, **9207**, 92070G.
- Koike, M. & Namioka, T. (2004). *AIP Conf. Proc.* **705**, 865–868.
- Lubeck, J., Beckhoff, B., Fliegau, R., Holfelder, I., Hönicke, P., Müller, M., Pollakowski, B., Reinhardt, F. & Weser, J. (2013). *Rev. Sci. Instrum.* **84**, 045106.
- Lukirskii, A. P. & Savinov, E. P. (1963). *Opt. Spectrosc.* **14**, 147–151.
- Maystre, D. & Petit, R. (1976). *Nouv. Rev. Opt.* **7**, 165–180.
- McEntaffer, R., DeRoo, C., Schultz, T., Gantner, B., Tutt, J., Holland, A., O'Dell, S., Gaskin, J., Kolodziejczak, J., Zhang, W. W., Chan, K.-W., Biskach, M., McClelland, R., Iazikov, D., Wang, X. & Koecher, L. (2013). *Exp. Astron.* **36**, 389–405.
- Mitzner, R., Neeb, M., Noll, T., Pontius, N. & Eberhardt, W. (2005). *Proc. SPIE*, **5920**, 59200D.
- Neviere, M., Maystre, D. & Hunter, W. R. (1978). *J. Opt. Soc. Am.* **68**, 1106–1113.
- Schnopper, H. W., Van Speybroeck, L. P., Delvaille, J. P., Epstein, A., Källne, E., Bachrach, R. Z., Dijkstra, J. & Lantward, L. (1977). *Appl. Opt.* **16**, 1088–1091.
- Werner, W. (1977). *Appl. Opt.* **16**, 2078–2081.
- Werner, W. & Visser, H. (1981). *Appl. Opt.* **20**, 487–492.